Ion release and tarnishing behavior of Au and Pd based amorphous alloys in artificial sweat

Ion Release and Tarnishing Behaviour of Au and Pd Based Amorphous Alloys in Artificial Sweat

Paola Rizzi[a*], Ingrid Corazzari[a], Gianluca Fiore[a], Ivana Fenoglio[a], Bice Fubini[a], Saulius Kaciulis[b], Livio Battezzati[a]

[a] Dipartimento di Chimica and NIS, Università di Torino, V. Giuria 7, 10125 Torino, Italy
[b] Institute for the Study of Nanostructured Materials, ISMN – CNR, PO Box 10, 00015 Monterotondo Stazione, Rome, Italy

* Corresponding author: Paola Rizzi, V. Giuria 7, 10125 Torino, Italy, paola.rizzi@unito.it Tel +390116707565 Fax +390112367565

Abstract

The corrosion resistance of Pd and Au based alloys in artificial sweat was studied using ICP-AES, XPS and SEM techniques. Amorphous ribbons were incubated for one week: the highest ion release was found for Au-based alloys, especially $Au_{49}Cu_{26.9}Ag_{5.5}Pd_{2.3}Si_{16.3}$, while in Pd-based alloys it was one order of magnitude less. The Ni released from $Pd_{32.5}Cu_{7.5}Ni_{40}P_{20}$ was below the limit imposed by the European regulation for objects in contact with skin. Major surface modification was detected after incubation of $Au_{49}Cu_{26.9}Ag_{5.5}Pd_{2.3}Si_{16.3}$, with formation of a nanoporous structure related to the observed tarnishing. Glassy alloys have higher corrosion resistance than the corresponding crystalline counterparts.

Keywords: A. alloy, B. ICP-OES, B. XPS, C. amorphous structures

1. Introduction

The study of glassy alloys based on precious metals started in the 1960s with the discovery of the first Au-Si metallic glass [1]. Only recently however, new formulations were developed by adding elements to the Au-Si system to improve the glass forming ability (GFA) and to enable the production of Au-based bulk metallic glasses having compositions close to 18 karats [2, 3, 4, 5]. Pd-based alloys are among the best bulk glass-formers and have been proposed for application as implants [6]. When the GFA and the undercooling range of the material are high enough, finished products can be made by forming in the undercooling regime to exploit the ability of the glassy alloy towards near-net-shape processing. Moreover, glassy alloys are reported to have good corrosion resistance, usually enhanced with respect to their crystalline counterparts [7, 8, 9, 10, 11, 12, 4]. The combined occurrence of both corrosion resistance and near-net-shape finish suggests the

application of Au and Pd based glassy metals in jewellery [2, 3, 4].

When new alloys are designed for use in jewellery, their possible toxicity has to be determined. Metallic objects in prolonged contact with skin may, in fact, exert a toxic effect generally attributed to the release of metal ions. The process is electrochemical in nature: electrons produced at the anode are consumed by the cathodic reaction during which, most commonly, oxygen reduction takes place. The metal ions formed in the anodic reaction are responsible for the toxic behaviour [13]. Ion release from a metal is strongly influenced by the standard electrode potentials and formation of passivation layers which could prevent further corrosion. Also the quantity, the composition and the electrolytic conductivity of the biologic fluid in contact with the metal play an important role in ion release [13, 14].

One consequence of metal ion toxicity is Allergic Contact Dermatitis (ACD) [15, 16]. Nickel allergy is the most frequent contact allergy in industrialized parts of the world [17, 18]. In order to prevent it, the presence of this metal and its release from objects intended to be in direct and prolonged contact with skin have been regulated by the Council Directive 94/27/EC stating that the Nickel release from such products must be less than 0.5 $\mu g\ cm^{-2}\ week^{-1}$ [19]. A standard procedure for determining the compliance to the European directive is based on the measurement of the concentration of Ni ions in artificial sweat solution after incubation for one week [20].

Even though allergy towards Au salts is well documented [21], the allergenic potential of metallic Gold is controversial as the scanty ion release, due to its chemical inertness, reduces the bioavailability of the ions necessary to elicit the allergic reaction [22]. Similarly, ACD has been observed after exposure to soluble Pd and Pt salts [13, 23]. Also in this case, the chemical inertness of these metals in their elemental state explains their limited relevance as sensitizers.

Despite the limited amount of evidences, Cu is increasingly recognized as an allergen. Even though it exhibits allergenic potential lower than other metals, it was observed that allergy to it, usually associated with allergy to Ni, has a certain clinical relevance [14].

Understanding the corrosion mechanism of amorphous alloys based on noble metals is increasingly important due to their possible applications that involve contact with body fluids, not only jewellery but also implants. In the former case also the possibility of tarnishing must be considered for aesthetic reasons. In this report, various Pd and Au based alloys are examined with the aim of determining their release of ions, corrosion resistance and tarnishing behaviour when immersed in an artificial sweat solution. The Pd-Cu-Si and Pd-Cu-Ni-P systems were chosen due to their high GFA. The Au-Cu-Si system with suitable additions was investigated being the basis for Au-based metallic glasses. Among these, the $Au_{49}Cu_{26.9}Ag_{5.5}Pd_{2.3}Si_{16.3}$ alloy appears the best glass-former to date and has been proposed for industrial applications [3]. Additions of Ti were made to Au-Cu-Si due to its ability to form passive layers. Finally, partially and fully crystalline samples were studied

to investigate the influence of the microstructure on the corrosion resistance.

2. Materials and methods

2.1. Synthesis, structural and microstructural characterisation

Au based ($Au_{44}Cu_{36}Ti_2Si_{18}$, $Au_{44}Cu_{37}Ti_1Si_{18}$, $Au_{42}Cu_{29}Ti_8Si_{21}$, $Au_{49}Cu_{26.9}Ag_{5.5}Pd_{2.3}Si_{16.3}$; atomic percentages) and Pd based ($Pd_{77.5}Cu_6Si_{16.5}$, $Pd_{72}Cu_{10}Si_{18}$, $Pd_{32.5}Cu_{7.5}Ni_{40}P_{20}$; atomic percentages) master alloys were prepared by arc melting suitable quantities of pure elements in an argon atmosphere. Lumps of the master ingots were then rapidly solidified by melt spinning in an Ar atmosphere. The structure of the as quenched ribbons was verified by X-Ray Diffraction (XRD) using Cu K_α radiation. The surface roughness was carefully examined by Scanning Electron Microscopy (SEM) before and after incubation in order to evidence possible preferential corrosion sites.

2.2. Ion release in artificial sweat

Ions release from amorphous ribbons of Au based and Pd based alloys and from crystalline Au based alloys was assessed following the reference test method for release of Nickel from products intended to come into direct and prolonged contact with skin developed by the European Committee for Standardization (CEN) prEN 1811 [20]. The artificial sweat [20, 24] was prepared by dissolving sodium chloride (0.5 wt. %), urea (0.1 wt, %) and lactic acid (0.1 wt. %) in aerated ultrapure Milli-Q water (Millipore, Bellerica, MA). The pH was adjusted to 6.5 with ammonia. The solution was employed within 3 h from preparation. Each alloy was cut to obtain samples of 1 cm^2 surface area. Samples were cleaned with ethanol in an ultrasonic bath for 5 minutes and then washed with ultrapure Milli-Q water. Each sample was immersed in 1 ml of artificial sweat in a plastic vial that was capped in order to prevent evaporation of the solution. The samples were then incubated at 30 ^oC for one week under static conditions. The same experimental procedure described above was carried out with a blank artificial sweat sample in the absence of the alloy. After incubation, the solution was diluted ten times with nitric acid 0.2 M. The ion content was analyzed by means of ICP-AES. In order to minimize metal trace contaminants, all glass and plastic objects used for the experiments were previously washed for 1 day with a 0.2 M nitric acid solution.

The crystalline samples examined as counterparts of amorphous ones, were part of the master ingot from which the amorphous ribbons were produced. They were in the form of regular parallelepipeds of 10 mm height, 5 mm width and 2 mm depth with a 1.6 cm^2 surface area. The surface was polished before incubation in order to avoid roughness due to the cut. Samples were immersed in 1.6 ml of artificial sweat and then the same incubation procedure was applied as described for the

amorphous ribbons.

All reagents were from Sigma Chemicals. All measurements were carried out in duplicate.

2.3. ICP-AES (Inductive Coupling Plasma – Atomic Emission Spectroscopy)

ICP-AES analyses of ions (Au, Ag, Cu, Si, Pd, Ti, Ni, P) were performed with an IRIS II Advantage/1000 Radial Plasma Spectrometer from Thermo-Jarrel Ash Corp. The optical system is sealed with an inert gas, has no moving parts, and is high resolution (ER/S) capable. The Echelle grating & Dispersion prism monochromator range is extended between 165 and 800 nm, with an optical resolution of 0.007 nm (at 200 nm). The photo device is a Charge Injection Device Camera cooled to -50 °C. The standard solutions of ions employed for the calibration of the instrument were prepared dissolving i) Merck CertiPUR ICP multi-element standard solution VIII and IV, ii) Merck Titrisol Silicon standard iii) Fluka Titanium atomic spectroscopy standard solution or iv) Na_3PO_4 in nitric acid 0.2 M. i) and ii) were from Merck Millipore (Darmstadt, Germany), iii) and iv) were from Sigma Aldrich, St. Louis, MO. The ion detection limits, expressed in ppb (by mass), in nitric acid solution (0.2 M) are reported in Table 1.

The data, expressed in μmol cm^{-2} $week^{-1}$, are the average of two separate experiments ± the Standard Error (SE).

2.4. XPS

The chemical composition of the samples surface was investigated by X-ray Photoelectron Spectroscopy (XPS), including also XPS depth profiling by means of cyclic Ar^+ ion sputtering. XPS measurements were carried out by using an ESCALAB MkII (VG Scientific) spectrometer, equipped with standard Al Kα excitation source and a 5-channeltron detection system. Two take-off angles (90° and 30°) were used for the variation of XPS information depth. These experiments were performed at a base pressure of about 1×10^{-8} Pa that was increased to 1×10^{-5} Pa during the depth profiling. The energy of the Ar^+ ion gun was set to 2.0 keV and the sample current density was about 2×10^{-3} mA/cm^2. The ion sputtering rate was calibrated by measuring reference samples (thin films of different metals on Si substrate) and applying the medium value of 0.3 nm/min [25, 26]. The binding energy (BE) scale was calibrated by setting the 1s peak of adventitious carbon (surface contamination) to BE = 285.0 eV and the Au $4f_{7/2}$ peak to BE = 84.0 eV. Further experimental details are reported elsewhere [25, 26].

3. Results

3.1. Structural, microstructural state and surface morphology

A detailed description of the structure and thermal stability of the rapidly solidified samples was

reported in previous publications and only a brief description is given in this section for the sake of comprehension. Ribbons of Pd based alloys ($Pd_{77.5}Cu_6Si_{16.5}$, $Pd_{72}Cu_{10}Si_{18}$, $Pd_{32.5}Cu_{7.5}Ni_{40}P_{20}$) [27] were confirmed to be amorphous using XRD. SEM analysis of surfaces excluded even isolated crystals. Analogously, the $Au_{49}Cu_{26.9}Ag_{5.5}Pd_{2.3}Si_{16.3}$ alloy [28] results completely amorphous when produced in ribbon form while $Au_{44}Cu_{37}Ti_1Si_{18}$, $Au_{44}Cu_{36}Ti_2Si_{18}$ and $Au_{42}Cu_{29}Ti_8Si_{21}$ [29] resulted partially crystalline to XRD and SEM analyses. The $Au_{42}Cu_{29}Ti_8Si_{21}$ ribbon shows a few precipitates on the side solidified in contact with the spinning wheel (wheel side), and a larger amount of precipitates embedded in the amorphous phase on the opposite side (air side) as can be seen in Fig 1a where an SEM backscattered image of the air side is presented. The precipitates contain Cu and Si, as determined by SEM/EDS analysis, and belong to a metastable cubic phase, $Cu_{15}Si_4$ type; moreover, Ti_5Si_3 crystals are also revealed by SEM although their reflections do not appear in the XRD patterns due to their low amount [30, 31]. $Au_{44}Cu_{36}Ti_2Si_{18}$ is amorphous on the wheel side, while a low amount of silicides is present on the air side. $Au_{44}Cu_{37}Ti_1Si_{18}$ is composed of an amorphous matrix in which a limited number of nanocrystals are embedded, appearing uniformly dispersed in the whole volume of the ribbon.

Typically, ribbons produced by melt spinning are characterised by a surface roughness due to the solidification conditions: the wheel side is irregular because of the roughness of the wheel with which the melt comes into contact and displays cavities caused by gas bubbles remaining entrapped between the liquid and the wheel during the quench; the opposite side (air side) shows only large undulations. As an example of the typical roughness of the ribbons produced by melt spinning, a SEM image of the $Pd_{72}Cu_{10}Si_{18}$ ribbon wheel side is presented in Fig. 1b, where a few cavities are indicated by arrows. On the air side of the $Pd_{72}Cu_{10}Si_{18}$ ribbon, an almost flat surface appears (Fig. 1 c).

3.2. Ion release in artificial sweat

After one week of incubation in artificial sweat, the solutions were analysed by means of ICP-AES and the results are reported in Fig. 2. In order to exclude any contamination due to impurities in the reagents or in the plastics and glassware employed, the ICP-AES analysis of the same ions was carried out on a blank solution of the artificial sweat (see Materials and Methods section) and none were detected in the solution.

The concentrations of Au, Ag, Pd and Si resulted to be below the detection limit in all solution samples which were analysed. The quantity of Cu released from $Pd_{77.5}Cu_6Si_{16.5}$ and $Pd_{72}Cu_{10}Si_{18}$ amorphous alloys was found to be similar and one order of magnitude less than that released from the quaternary Au based alloys ($Au_{44}Cu_{37}Ti_1Si_{18,}$ $Au_{44}Cu_{36}Ti_2Si_{18}$ and $Au_{42}Cu_{29}Ti_8Si_{21}$), which liberate also small amounts of Ti. The largest quantity of Cu was released by the

$Au_{49}Cu_{26.9}Ag_{5.5}Pd_{2.3}Si_{16.3}$ alloy (Fig. 2). The Cu release is not proportional to its content in the alloys, showing that factors other than composition influence the stability of the alloys in artificial sweat.

When $Pd_{32.5}Cu_{7.5}Ni_{40}P_{20}$ ribbons were incubated, Cu was not revealed in the solution, whilst both Phosphorus and Nickel were detected. The amount of Ni released from this alloy (0.00165 μmol cm^{-2} $week^{-1}$), was below the limit imposed by the European regulation for objects which come in direct and prolonged contact with skin [19].

The release of Ti from the Au based amorphous alloys (Fig. 2) is inversely proportional to its content in the alloy, so that $Au_{42}Cu_{29}Ti_8Si_{21}$ has the lowest amount of Ti ion released.

The results obtained for Au-based amorphous alloys were compared with those obtained for crystalline samples having the same overall composition and constituted by mixtures of phases ($Au_{44}Cu_{37}Ti_1Si_{18}$, $Au_{44}Cu_{36}Ti_2Si_{18}$ and $Au_{49}Cu_{26.9}Ag_{5.5}Pd_{2.3}Si_{16.3}$). Fig 3 shows that amorphous ribbons release lower amounts of ions in artificial sweat than the corresponding crystalline samples. The difference between amorphous and crystalline alloys is more pronounced for $Au_{44}Cu_{37}Ti_1Si_{18}$ and $Au_{44}Cu_{36}Ti_2Si_{18}$, as revealed by the amount of Cu and Ti found in the solution. Moreover, when crystalline $Au_{49}Cu_{26.9}Ag_{5.5}Pd_{2.3}Si_{16.3}$ is incubated, the release of Pd was revealed by ICP, whereas this element was not dissolved when amorphous samples were tested.

From the released quantities reported in Fig. 2 it is possible to estimate an approximate thickness of the modified surface layer leached during incubation. This can be obtained from the alloy density and assuming that the atoms are all released from the surface of the ribbons of known area. The result is that leaching occurs down to a depth of a few nm for Pd-based alloys and to less than 10 nm for Au-based alloys except for the $Au_{49}Cu_{26.9}Ag_{5.5}Pd_{2.3}Si_{16.3}$ alloy where the depth reaches about 100 nm.

3.3. Surface modification

Before incubation in artificial sweat, apart from the roughness described in section 3.1., the surface is smooth and similar for all Au and Pd alloys (see Fig. 1b and Fig. 1 c for $Pd_{72}Cu_{10}Si_{18}$). After incubation, SEM observations of Pd based ribbons did not show any change in surface morphology except for the $Pd_{72}Cu_{10}Si_{18}$ alloy where the presence of a limited number of crystals with diameter of about 100 nm was revealed on the air side (Fig. 4a). Also the SEM analysis of $Au_{44}Cu_{37}Ti_1Si_{18}$ and $Au_{44}Cu_{36}Ti_2Si_{18}$ did not evidence any change in surface morphology on the air side, while on the wheel side a limited number of crystals was observed. After incubation, the air side of $Au_{49}Cu_{26.9}Ag_{5.5}Pd_{2.3}Si_{16.3}$ was strongly modified, with the formation of crystals covering the entire surface, with diameters of about 100 nm (Fig. 4c). An X ray diffraction analysis in parallel beam configuration showed on the air side reflections of an fcc phase rich in gold having scattering

domains of a few nanometres. Moreover, an XPS analysis revealed the occurrence of SiO_2 together with Au [25]. Since the particles on the surface are about 100 nm in size (from SEM observations), it can be surmised these particles are aggregates of both components. Similarly, particles of about 50 nm diameter were formed after incubation on the $Au_{42}Cu_{29}Ti_8Si_{21}$ air side (Fig. 4b).

3.4. XPS analyses

A composition gradient was observed on both sides of the as produced $Pd_{77.5}Cu_6Si_{16.5}$ ribbons, with segregation of Si that forms SiO_2 and silicide traces not detectable by XRD (Fig 5 a and Fig 5 b for wheel and air side, respectively). This can be explained by the reaction with the residual oxygen unavoidably present in the quenching chamber despite repeated evacuations. The Si amount rapidly decreases and, at the depth of about 4 nm, the nominal composition is reached for both sides. A similar trend was observed for the as quenched $Pd_{72}Cu_{10}Si_{18}$ sample that shows Si segregation on the surface. The nominal composition is reached at the depth of about 3 nm.

After treatment in artificial sweat, a limited modification of the surface composition with respect to the as quenched ribbons was found for the $Pd_{77.5}Cu_6Si_{16.5}$ sample (Fig. 5, c and d for wheel and air side, respectively) where the presence of nitrogen can be associated with the urea contained in the artificial sweat solution. The Si segregation on the surface remains almost unchanged and the nominal composition is reached at the depth of about 4 nm. Instead, a slight difference between the air and wheel side of $Pd_{72}Cu_{10}Si_{18}$ was revealed after incubation. On the wheel surface, smaller amounts of SiO_2 and silicide traces are found with respect to the air side and the nominal composition is reached at about 3.5 nm. Also for this sample, the presence of N can be associated with the artificial sweat solution.

The melt-spun $Au_{44}Cu_{37}Ti_1Si_{18}$ ribbon before incubation appears to have different composition depending on the side examined: on the wheel side (Fig. 6 a) an enrichment in Si and Cu is found, most likely due to a preferential oxidation occurred during the solidification. The resulting oxidized layer is about 30 nm thick. On the air side (Fig. 6 b) an enrichment in Cu and Si is found, but the thickness of the layer is limited to about 2 nm. After the incubation in artificial sweat, Ti is not found anymore on the surfaces, probably because it was leached. On the wheel side an enrichment in Cu occurs down to 6 nm. On the air side, there is an enrichment in Cu on the very extreme surface (<1 nm) and after 15 nm the nominal composition is reached.

In previous studies on $Au_{49}Cu_{26.9}Ag_{5.5}Pd_{2.3}Si_{16.3}$, [25] XPS analysis revealed different compositions on the two ribbon sides before incubation: the air side is almost completely covered by an SiO_2 layer a few nanometers thick and on the wheel side Cu and Si are preferentially segregated on the surface. After incubation, on the air side, a thick layer of at least 70 nm was revealed, composed only of gold and SiO_2.

4. Discussion

Four aspects are considered in our discussion of results: i) leaching of elements and solid oxide formation during incubation; ii) surface modification that produces tarnishing of precious amorphous alloys; iii) corrosion resistance of the amorphous ribbons with respect to the crystalline master alloys; iv) biocompatibility.

4.1. Leaching and solid oxide formation

From the results on surface analyses and ions release, it is apparent that components of the amorphous alloys are either leached or oxidised to solid compounds. This result can be mostly understood by considering the equilibrium potentials of elements together with passivation effects.

It must be stressed that an amorphous alloy is metastable and, therefore, the chemical and electrochemical potentials of elements in it are affected by its free energy being higher than that of the corresponding equilibrium phases. Note, however, that extensive studies on the thermodynamics of crystallisation have shown that the free energy change upon crystallisation is of the order of one third - one half the heat of fusion, i.e. in most cases it amounts to a few units in kJ/mol [32]. The alloys dealt with here can be regarded as amorphous silicides, therefore, their stability is chiefly determined by the free energy of formation of silicides. As a consequence, they are chemically and electrochemically stabilised with respect to the constituting elements, apart from galvanic effects. Therefore, a guide to the oxidation behaviour of elements is provided to a first approximation by their equilibrium potentials. Since the as-prepared artificial sweat is slightly acidic (pH 6.5), the formation of SiO_2 can be inferred from Pourbaix diagrams [33], similarly to $Au_{49}Cu_{26.9}Ag_{5.5}Pd_{2.3}Si_{16.3}$ where the presence of SiO_2 was evidenced by XPS after incubation [25].

XPS results on Pd based ribbons revealed that a layer of a few nanometers is formed on the surface during rapid solidification, mainly containing SiO_2. This layer contributes to the passivation of the surface. This phenomenon is reported in the literature for other metallic glasses for which the formation of a passive film in air is revealed by means of different analytical studies [34]. During incubation, it can be expected that pitting corrosion starts from the imperfections present on the surface such as cavities, roughness, inclusions and precipitates where the passive layer can be more easily broken or galvanic effects be operative [11]. Moreover, the Pourbaix diagram of the copper-chlorine-water system shows that the presence of chloride in solution promotes the dissolution of Cu during free corrosion over a wide range of pH with the formation of $CuCl_2^-$ species. This is in agreement with the ICP-AES results that show the presence of Cu in solution after incubation.

For Cu-Ni crystalline alloys in sodium chloride solutions, it is reported that [35, 36, 34], when Ni is present in the alloy in higher content than Cu, it oxidised preferentially. A similar behaviour is

found in amorphous alloys containing Ni in excess with respect to Cu (e. g. $Pd_{32.5}Cu_{7.5}Ni_{40}P_{20}$).

For the Au based alloys containing Ti ($Au_{44}Cu_{37}Ti_1Si_{18}$, $Au_{44}Cu_{36}Ti_2Si_{18}$, $Au_{42}Cu_{29}Ti_8Si_{21}$) two issues must be taken into account: i) the passivating action of Ti that most likely forms Ti oxides on the surface in view of its highly negative equilibrium potential; ii) the presence of inclusions and precipitates that can promote pitting corrosion of either the precipitate itself or of the neighbouring phase. For the former issue, an increasing corrosion resistance can be expected by increasing the amount of Ti in the alloy. Increasing the amount of Ti in the alloy, on the contrary, decreases the glass forming ability of the system and crystalline phases are produced next to the amorphous one. Therefore, the corrosion resistance of the Ti containing alloys can be considered as a balance of opposed contributions. In $Au_{44}Cu_{37}Ti_1Si_{18}$ the Ti content is too low to form an effective passive layer. In $Au_{44}Cu_{36}Ti_2Si_{18}$ and $Au_{42}Cu_{29}Ti_8Si_{21}$ the amorphous matrix coexists with a metastable Cu-rich silicide and Ti_5Si_3 crystals. Ti is incorporated in large amounts in such highly stable compounds which will very likely contribute to passivation. These considerations are confirmed by the behaviour of crystalline alloys ($Au_{44}Cu_{37}Ti_1Si_{18}$, $Au_{44}Cu_{36}Ti_2Si_{18}$, in Fig. 3) containing a Au-Cu solid solution, Ti_5Si_3 and a Cu rich silicide: here also Ti is released together with an amount of Cu.

4.2. Tarnishing behaviour

When ribbons are incubated for one week, a tarnishing of the surface is observed for some compositions by visual observation. This is related to a chemical and morphological change of the surface due to leaching or oxide formation.

The incubation in artificial sweat can be intended as the first stage of a dealloying process. As described in the literature for dealloying of amorphous metals [30, 31, 37, 38], when dissolution occurs, noble adatoms remain on the surface being highly mobile because of surface diffusion. Since the local composition drops quickly outside the amorphisation range of the system, a consequent crystallisation of the amorphous matrix takes place with formation of crystals constituted by the more noble elements in the alloy. The size of crystals - or aggregates of crystals - and thickness of sample involved in dealloying are proportional to the amount of ions released. Therefore, the change in composition of $Au_{49}Cu_{26.9}Ag_{5.5}Pd_{2.3}Si_{16.3}$ due to both Cu loss and Si oxidation, leaves on the surface fine crystals made of noble elements with high reciprocal solubility (Au, Ag, Pd). The leaching results in the formation of a thick porous layer. As reported in the literature, the colour of nanoporous gold is affected by the surface morphology so that a range of colours from deep red to black gold can be obtained by tailoring the dimension of pores and ligaments [39, 40]. Therefore, the tarnishing observed after incubation in artificial sweat can be connected to the formation of a nanoporous structure on the surface of the material. The tarnishing effect will be more visible depending on the dimension of pores and hillocks formed on the surface

and on the thickness of the nanoporous layer. In this respect, a more limited tarnishing was observed for $Au_{42}Cu_{29}Ti_8Si_{21}$ where SEM analysis shows the presence of a thinner nanoporous structure (Fig. 4b) with a morphology similar to $Au_{49}Cu_{26.9}Ag_{5.5}Pd_{2.3}Si_{16.3}$ alloy. Tarnishing was not observed for the other alloys in which the surface remained almost flat after incubation.

4.3. Corrosion resistance

In order to determine the corrosion resistance of the amorphous ribbons with respect to the crystalline alloys, the ion released from the amorphous ribbons was compared to that of the master alloys and the result is reported in Fig. 3. The crystalline samples were polished before the incubation in order to have smooth surfaces. Moreover, the parallelepiped shape was chosen in order to have similar shapes for both samples. In Fig. 3 it is evident that higher amounts of ions are released by crystalline alloys.

Crystalline metals contain grain boundaries and different phases that can form micro-galvanic cells enhancing the corrosion rate. In glassy alloys the composition is homogeneous in the whole sample and grain boundaries are absent; therefore, corrosion starts usually from imperfections on the sample surface. When samples contain crystalline fractions, the crystals usually induce corrosive attack. As for the samples studied in this research, in the case of $Au_{44}Cu_{37}Ti_1Si_{18}$ master alloy, XPS revealed that Ti is no longer present on the sample surface, so that the leaching of the crystalline phase containing Ti can be envisaged, due to the formation of galvanic cells between the Au containing crystalline phases (most likely with higher equilibrium potentials) and silicides. For the $Au_{44}Cu_{36}Ti_2Si_{18}$ ribbon the partially crystalline air side acts as anode in the galvanic cell and promotes the dissolution from one ribbon side. This effect does not occur when the almost fully amorphous $Au_{44}Cu_{37}Ti_1Si_{18}$ ribbon or the partially crystalline $Au_{42}Cu_{29}Ti_8Si_{21}$ are considered, having similar structures on both sides. Moreover, in $Au_{42}Cu_{29}Ti_8Si_{21}$ the presence of Ti silicides contribute to the passivation of the surface.

4.4. Biocompatibility aspects

The amount of Ni^{2+} ions released from the $Pd_{32.5}Cu_{7.5}Ni_{40}P_{20}$ amorphous ribbons after incubation in artificial sweat (0.00165 μmol cm^{-2} $week^{-1}$) is largely below the limit imposed by the European Directive [19]. In this sense, despite the presence of Ni, the $Pd_{32.5}Cu_{7.5}Ni_{40}P_{20}$ alloy can be regarded as a material suited for the production of objects to be used in contact with skin. A precise threshold value of concentration below which no allergenic response is exerted, has not yet been assessed for Cu, as it depends upon many factors such as duration of the exposure, pre-existing inflammatory reactions of the skin, extension of the skin area exposed, gender and age [41]. The amount of Cu released from Au based alloys found in this research, might represent a contribution in case

regulations will be issued in future.

5. Conclusions

The corrosion resistance in artificial sweat of Au- and Pd-based amorphous and crystalline alloys has been studied by means of various experimental techniques, in order to evaluate a possible use of precious amorphous alloys in applications in contact with skin. When compared with the corresponding crystalline alloys, amorphous alloys show a stronger corrosion resistance as testified by ICP-AES analyses that evidenced a larger amount of ions released by crystalline samples. Moreover, when Ni is present in the material (e. g. $Pd_{32.5}Cu_{7.5}Ni_{40}P_{20}$ amorphous ribbons) the amount of Ni^{2+} ions released in artificial sweat is 0.00165 μmol cm^{-2} $week^{-1}$, value largely below the limit imposed by the European Directive (94/27/EEC, 1994).

During incubation, tarnishing -i.e. the change in colour of the surface - was evidenced for some compositions, especially the good glass-former $Au_{49}Cu_{26.9}Ag_{5.5}Pd_{2.3}Si_{16.3}$. This casts doubt on its potential use in jewellery unless further additives are found to passivate it. The tarnishing could be explained in terms of a de-alloying process with formation of a nanoporous structure and crystallization of the noble component of the alloy. A passivation effect was observed in Au based alloys containing Ti in which the increase in Ti content corresponds to a decrease in surface leaching.

Acknowledgements

Work performed has been for Ateneo-Compagnia di San Paolo-2011-Linea 1A, project ORTO11RRT5. Fondazione S. Paolo is acknowledged for support to CdE NIS

References

[1] W.Klement, RH.Willens, P.Duwez, Non-crystalline structure in solidified Gold-Silicon alloys, Nature 187 (1960) 869-870

[2] J. Schroers, B. Lohwongwatana, W.L. Johnson, A. Peker, Gold based bulk metallic glass, Appl. Phys. Lett. 87 (2005) 061912

[3] J. Schroers, B. Lohwongwatana, W.L. Johnson, A. Peker, Precious bulk metallic glasses for jewelry applications, Mater. Sci. Eng. A 448 (2007) 235–238

[4] S. Mozgovoy, J. Heinrich, U.E. Klotz, R. Busch, Investigation of mechanical, corrosion and optical properties of an 18 carat Au-Cu-Si-Ag-Pd bulk metallic glass, Intermetallics 18 (2010) 2289-2291

[5] G. Fiore, P. Rizzi, L. Battezzati, Phase constitution and glass formation in an Au-based alloy, J. Alloy Compd., 509S (2011) S166–S169

[6] M.D. Demetriou, M.E. Launey, G. Garrett, J.P. Schramm, D.C. Hofmann, W.L. Johnson, R.O. Ritchie, A damage-tolerant glass, Nat. Mater. 10 (2011) 123-128

[7] A. Inoue, Stabilization of metallic supercooled liquid and bulk amorphous alloys, Acta Mater. 48 (2000) 279-306

[8] K.Hashimoto, Chemical properties, in: F.Luborsky (Ed.) Amorphous metallic alloys, Butterworth & Co. London, 1983, p. 471

[9] W.H Peter, R.A Buchanan, C.T Liu, P.K Liaw, M.L Morrison, J.A Horton, C.A Carmichael Jr., J.L Wright, Localized corrosion behavior of a zirconium-based bulk metallic glass relative to its crystalline state, Intermetallics 10 (2002) 1157–1162

[10] B.R.Bernard, P.K.Liaw, M.D.Demetriou, W.L.Johnson, Oxidation of metallic glass foams, Corros. Sci., 50 (2008) 2135-2139

[11] A.Gebert, P.F.Gostin, L.Schultz, Effect of surface finishing of a Zr-based bulk metallic glass on its corrosion behaviour, Corros. Sci., 52 (2012) 1711-1720

[12] S.Pang, C.Shek, T.Zhang, K.Asami, A.Inoue, Corros. Sci., 48 (2006) 625-633

[13] G N.Flint, A metallurgical approach to metal contact dermatitis, Contact Dermatitis, 39 (1998) 213-221

[14] J.J.Hostynek, H.I.Maibach Copper hypersensitivity: dermatologic aspects, Dermatol. Ther. 17(4) (2004) 328-33.

[15] T.Fischer, Occupational nickel dermatitis. In: Maibach HI, Menne T. (eds): Nickel and the skin: immunology and toxicology, Boca Raton, Fl, USA, CRC Press, (1989) 117

[16] J.W.Cherrie, A.Robertson, Biologically relevant assessment of dermal exposure, Ann. Occup. Hyg. 39 (1995) 387–391

[17] C.Lidén, S.Carter, Nickel release from coins, Contact Dermatitis 44 (2001) 160–165

[18] L.Büdinger, M.Hertl, Immunologic mechanisms in hypersensitivity reactions to metal ions: an overview, Allergy 55 (2000) 108-115

[19] European Directive, 94/27/EC, (1994)

[20] European Committee for Standardization (CEN). Reference test method for release of nickel from products intended to come into direct and prolonged contact with the skin UNI prEN 1811, (1998)

[21] H.Möller, Dental gold alloys and contact allergy, Contact Dermatitis 47 (2002) 63–66

[22] C.Lidén, M.Nordenadler, L.SKARE Metal release from gold-containing jewellery materials: no gold release detected, Contact Dermatitis, 39 (1998) 281

[23] L.A.Garner, Contact dermatitis to metals, Dermatol. Ther., 17 (2004) 321–327

[24] S. Colin, E.Beche, R.Berjoan, H.Jolibois, A.Chambaudet, An XPS and AES study of the free corrosion of Cu-, Ni- and Zn-based alloys in synthetic sweat, Corros. Sci., 41 (1999) 1051 - 1065

[25] S.Kaciulis, A.Mezzi, G.Fiore, I.Ichim, L.Battezzati, P.Rizzi, XPS study of gold-basedmetallic glass, Surf. Interface Anal., DOI 10.1002/sia.3231, 42 (2010) 597–600

[26] E. Agostinelli, S. Kaciulis, M. Vittori-Antisari, Great reduction of particulates in pulsed laser deposition of Ag-Co films by using a shaded off-axis geometry, Appl. Surf. Sci., 156 (2000) 143-148

[27] G.Fiore, L.Battezzati, Thermodynamic properties of the $Pd_{77.5}Cu_6Si_{16.5}$ undercooled liquid, J. Alloys Compd., 483 (2009) 54–56

[28] G. Fiore, I. Ichim, L. Battezzati, Thermal analysis, fragility and viscosity of Au-based metallic glasses, J. Non-Cryst. Solids 356 (2010) 2218

[29] G. Fiore, L.Battezzati, Developing Au-based amorphous alloys, Rev. Adv. Mater. Sci. 18 (2008) 190-192

[30] F. Scaglione, A.Gebert, L. Battezzati, Dealloying of an Au-based amorphous alloy, Intermetallics 18 (2010) 2338-2342

[31] L.Battezzati., F.Scaglione, De-alloying of rapidly solidified amorphous and crystalline alloys, J. Alloys Compd., 509S (2011) S8–S12

[32] R.W. Cahn, A.L. Greer, Metastable States of Alloys, in: Physical Metallurgy, Robert W. Cahn and Peter Haasen (Ed.) Elsevier Science, Amsterdam (1996) 1723-1830 and references therein.

[33] M. Pourbaix, Atlas d'équilibres électrochimiques à 25°C, Gauthier-Villars & C. ed., Paris, (1963) 461

[34] S.Colin, E.Beche, R.Berjoan, H.Jolibois, A.Chambaudet, An XPS and AES study of the free corrosion of Cu-, Ni, and Zn-based alloys in synthetic sweat, Corros. Sci., 41 (1999) 1051 - 1065

[35] R.G.Blundy, M.J.Pryor, The potential dependence of reaction product composition on copper-nickel alloys, Corros. Sci. 12 (1972) 65-75

[36] W.A.Badawy, K.M. Ismail, A.M. Fathi, Effect of Ni content on the corrosion behavior of Cu–Ni alloys in neutral chloride solutions, Electrochimica Acta 50 (2005) 3603–3608

[37] J.Yu , Y.Ding, C.Xu, A.Inoue, T.Sakurai, M.Chen, Nanoporous metals by dealloying multicomponent metallic glasses, Chem. Mater. 20 (2008) 4548-4550.

[38] H.Abe, K.Sato, H.Nishikawa, T.Takemoto, M. Fukuhara, A. Inoue, Dealloying of Cu-Zr-Ti bulk metallic glass in hydrofluoric acid solution, Mater. Trans. 50 (2009) 1255-1258

[39] F.Kertis, J.Snyder, L.Govada, S.Khurshid, N.Chayen, J.Erlebacher, Structure/processing relationships in the fabrication of nanoporous gold, JOM, 62 (2010) 50-56

[40] K.Nishio, H.Masuda, Anodization of gold in oxalate solution to form a nanoporous black film, Angew. Chem. Int. Ed. 50 (2011) 1603-1607
[41] D.A.Basketter, P.Evans, G.F.Gerberick, I.A.N. Kimber, Factors affecting thresholds in allergic contact dermatitis: safety and regulatory considerations, Contact Dermatitis 47 (2002) 1–6

Figure captions

Fig. 1: SEM images of: a) $Au_{42}Cu_{29}Ti_8Si_{21}$ ribbons air side before incubation, backscattered electrons image; b) $Pd_{72}Cu_{10}Si_{18}$ ribbons wheel side before incubation, secondary electrons image; cavities are indicated by arrows; c) $Pd_{72}Cu_{10}Si_{18}$ ribbons air side before incubation, secondary electrons image.

Fig. 2: ICP-AES ion release from samples analyzed after one week of incubation in artificial sweat. Au, Ag, Pd and Si were always under the detection limit and, therefore, are not reported in figure.

Fig. 3: ICP-AES ion release from $Au_{44}Cu_{37}Ti_1Si_{18}$, $Au_{44}Cu_{36}Ti_2Si_{18}$, $Au_{49}Cu_{26.9}Ag_{5.5}Pd_{2.3}Si_{16}$ alloys analyzed after one week of incubation in artificial sweat: a) amorphous ribbons and b) crystalline alloys. Au, Ag, Pd and Si were always under the detection limit and, therefore, are not reported in figure.

Fig. 4: SEM images of ribbon surfaces of a) $Pd_{72}Cu_{10}Si_{18}$, b) $Au_{42}Cu_{29}Ti_8Si_{21}$ and (c) $Au_{49}Cu_{26.9}Ag_{5.5}Pd_{2.3}Si_{16}$ after one week of incubation in the artificial sweat solution.

Fig. 5: XPS depth profiles of $Pd_{77.5}Cu_6Si_{16.5}$ ribbons: a) wheel side before incubation; b) air side before incubation; c) wheel side after incubation; d) air side after incubation.

Fig. 6: XPS depth profiles of $Au_{44}Cu_{37}Ti_1Si_{18}$ ribbons before incubation: a) wheel side; b) air side.

Table 1: Detection limits of the ions analyzed by ICP-AES in nitric acid solution (0.2 M) expressed in ppb (by mass).

Figure 1a

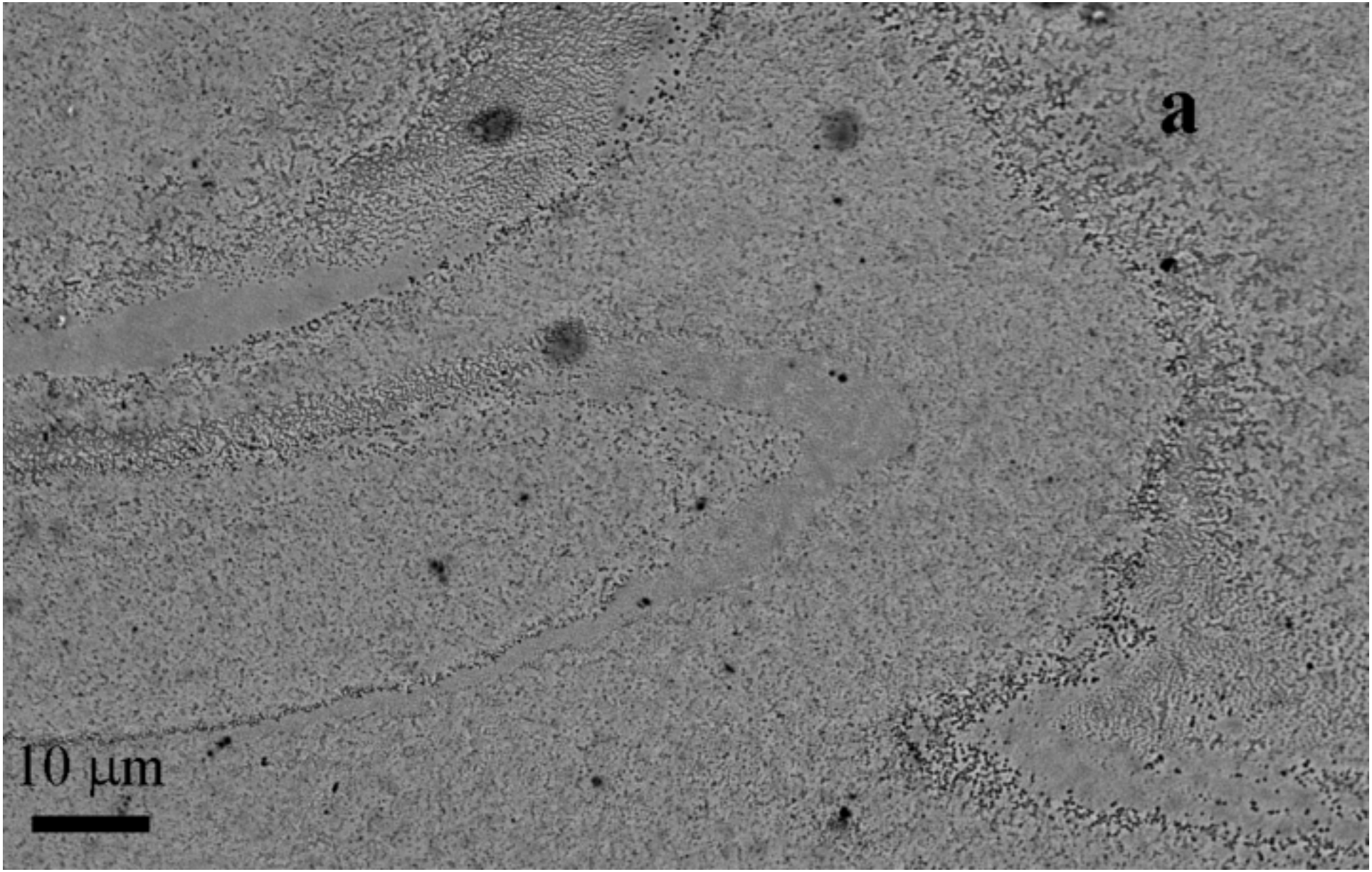

Figure 1 b

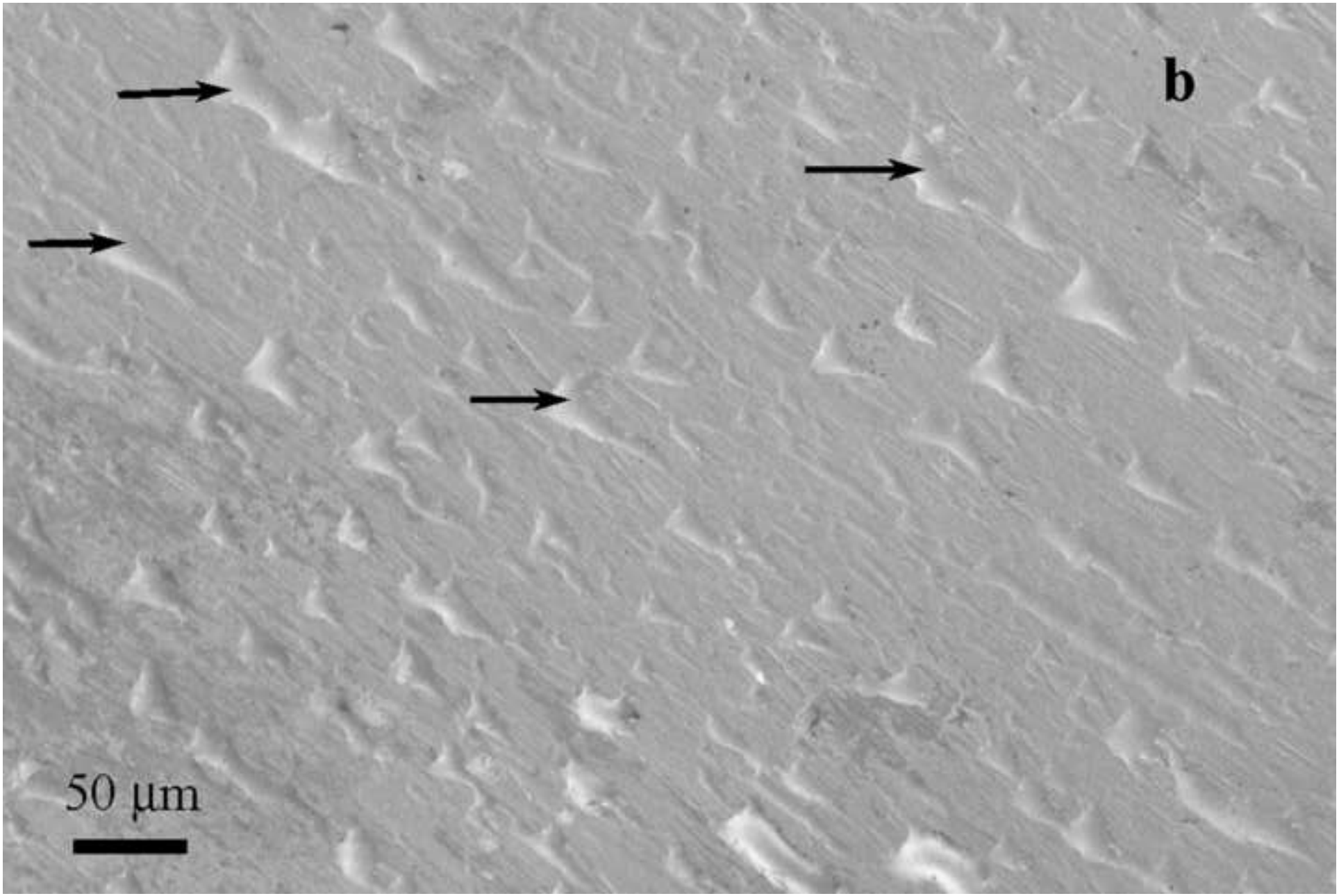

Figure 1c

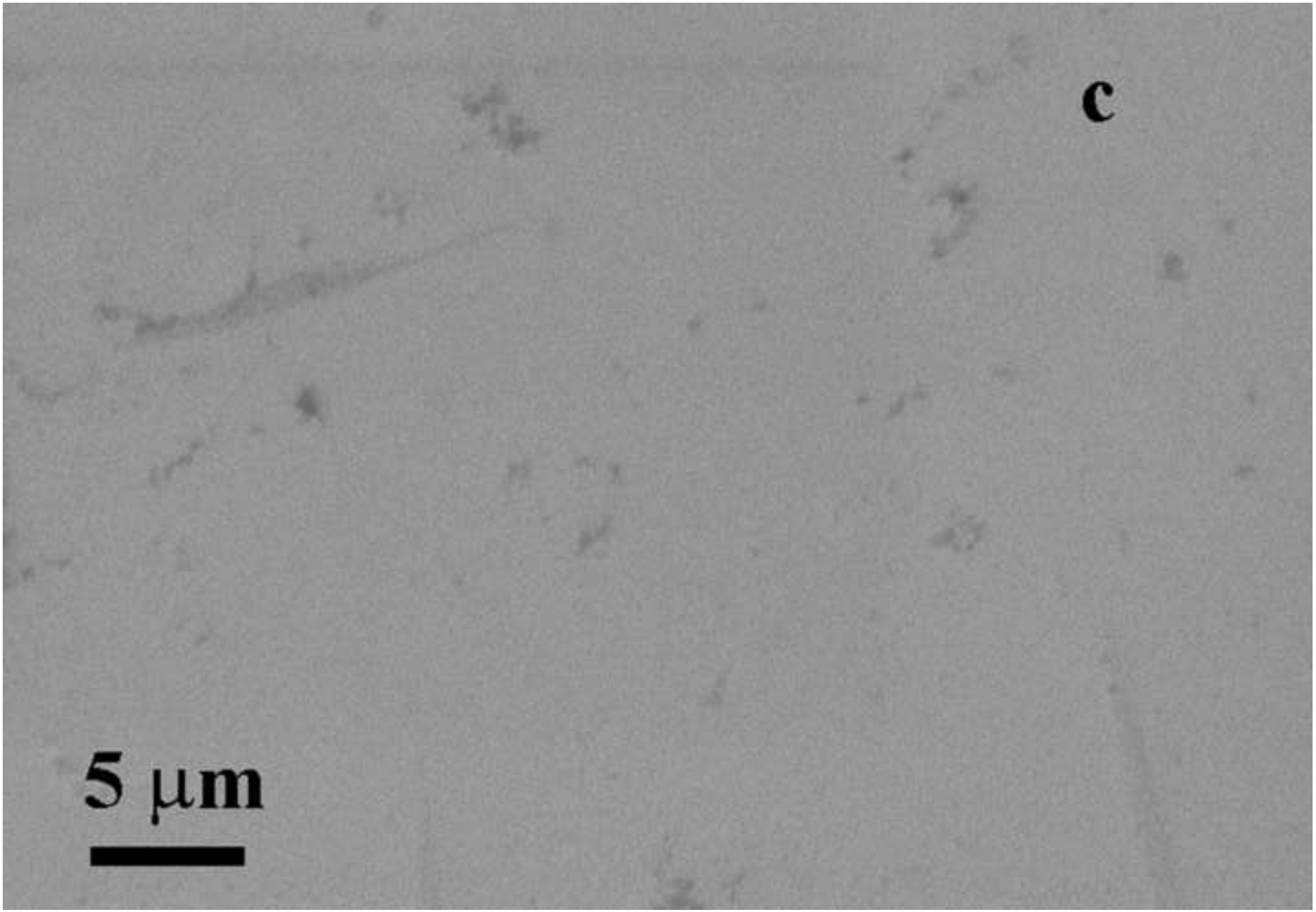

Figure 2

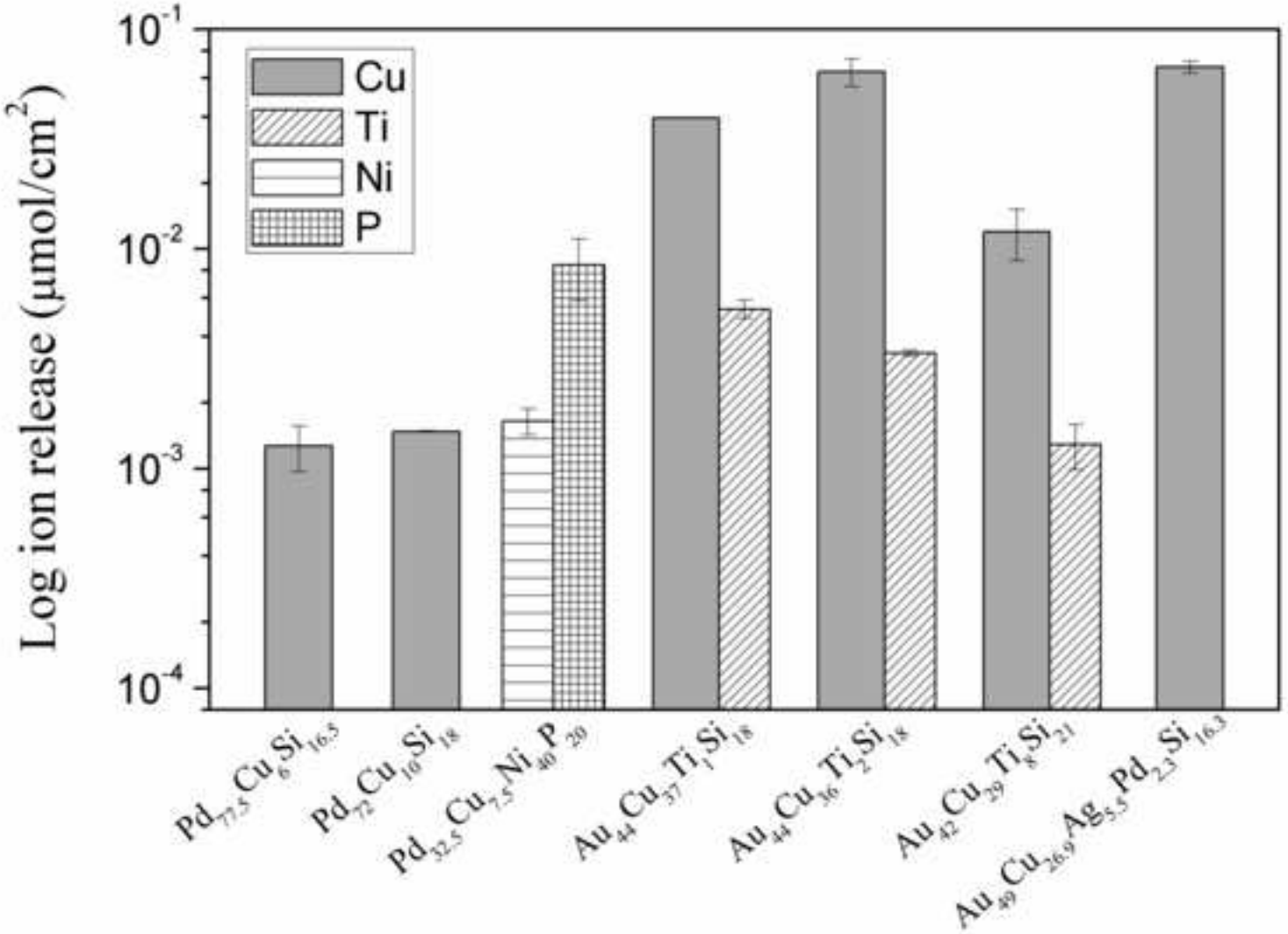
Log ion release (μmol/cm²)
10⁻¹
10⁻²
10⁻³
10⁻⁴
Cu
Ti
Ni
P
Pd77.5Cu6Si16.5
Pd72Cu10Si18
Pd32.5Cu7.5Ni40P20
Au44Cu37Ti1Si18
Au44Cu36Ti2Si18
Au42Cu29Ti8Si21
Au49Cu26.9Ag5.5Pd2.3Si16.3

Figure 3

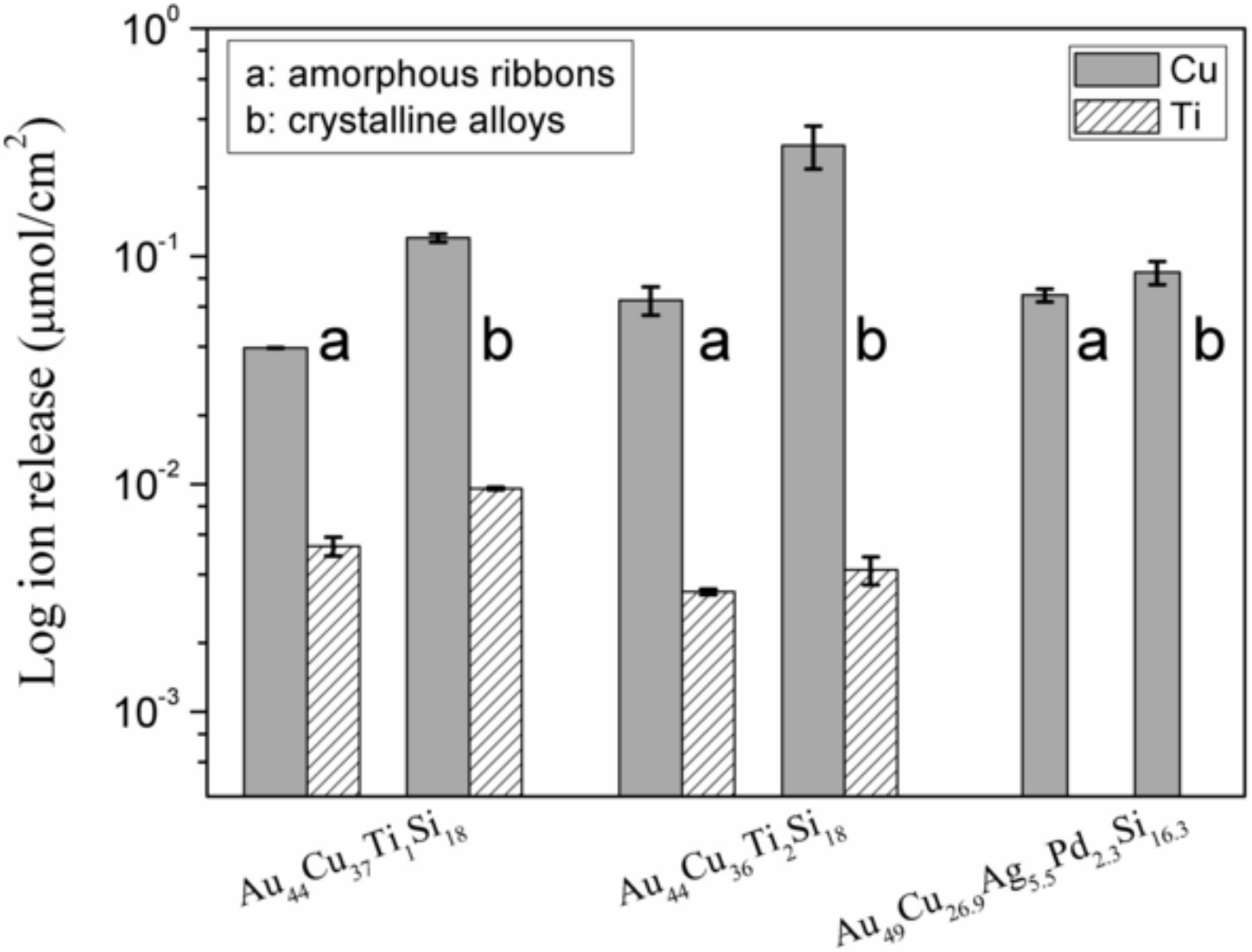
a: amorphous ribbons
b: crystalline alloys
Cu
Ti
Log ion release (μmol/cm²)
10⁰
10⁻¹
10⁻²
10⁻³
a
b
a
b
a
b
Au44Cu37Ti1Si18
Au44Cu36Ti2Si18
Au49Cu26.9Ag5.5Pd2.3Si16.3

Figure 4a

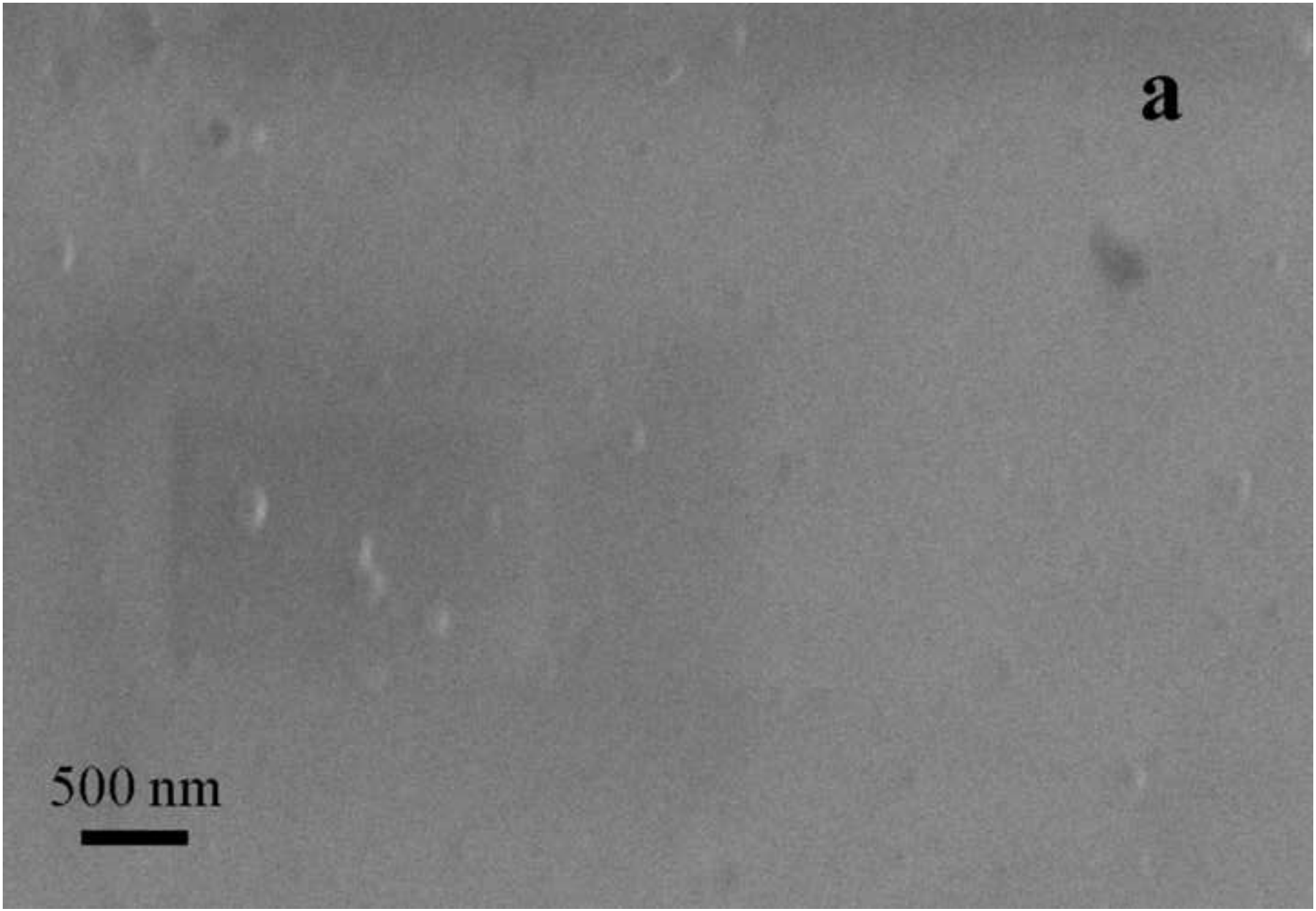

Figure 4b

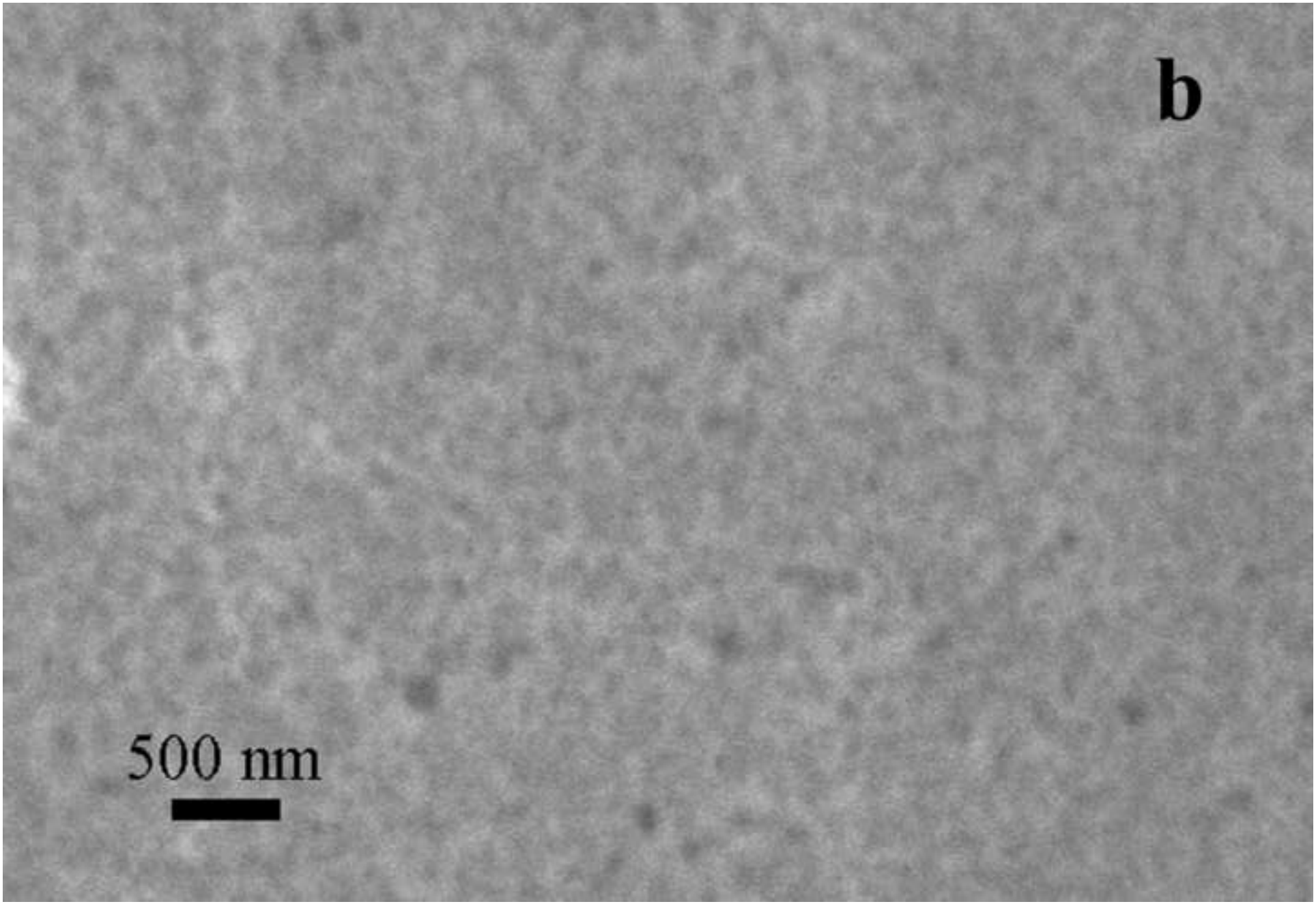

Figure 4c

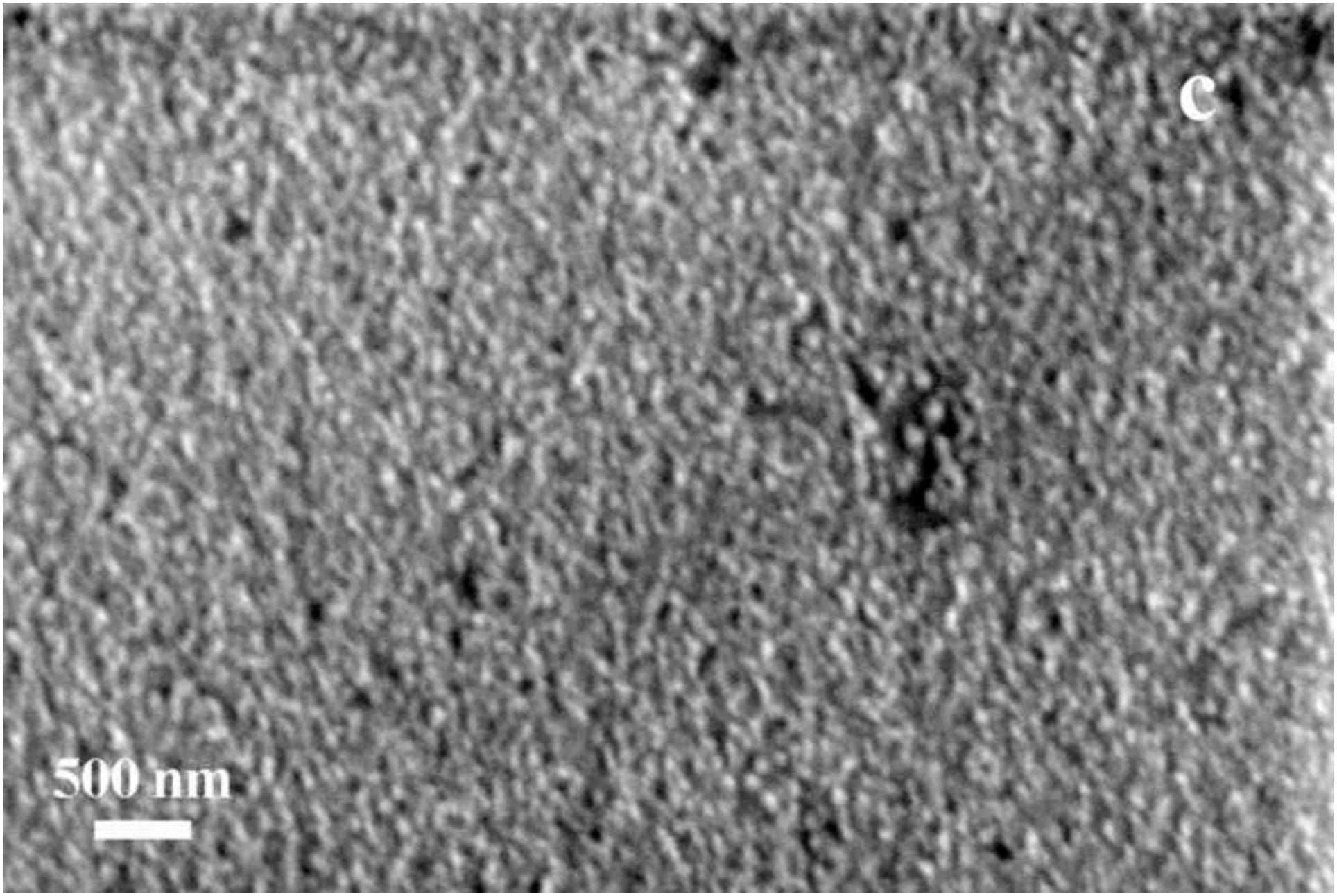

Figure 5a

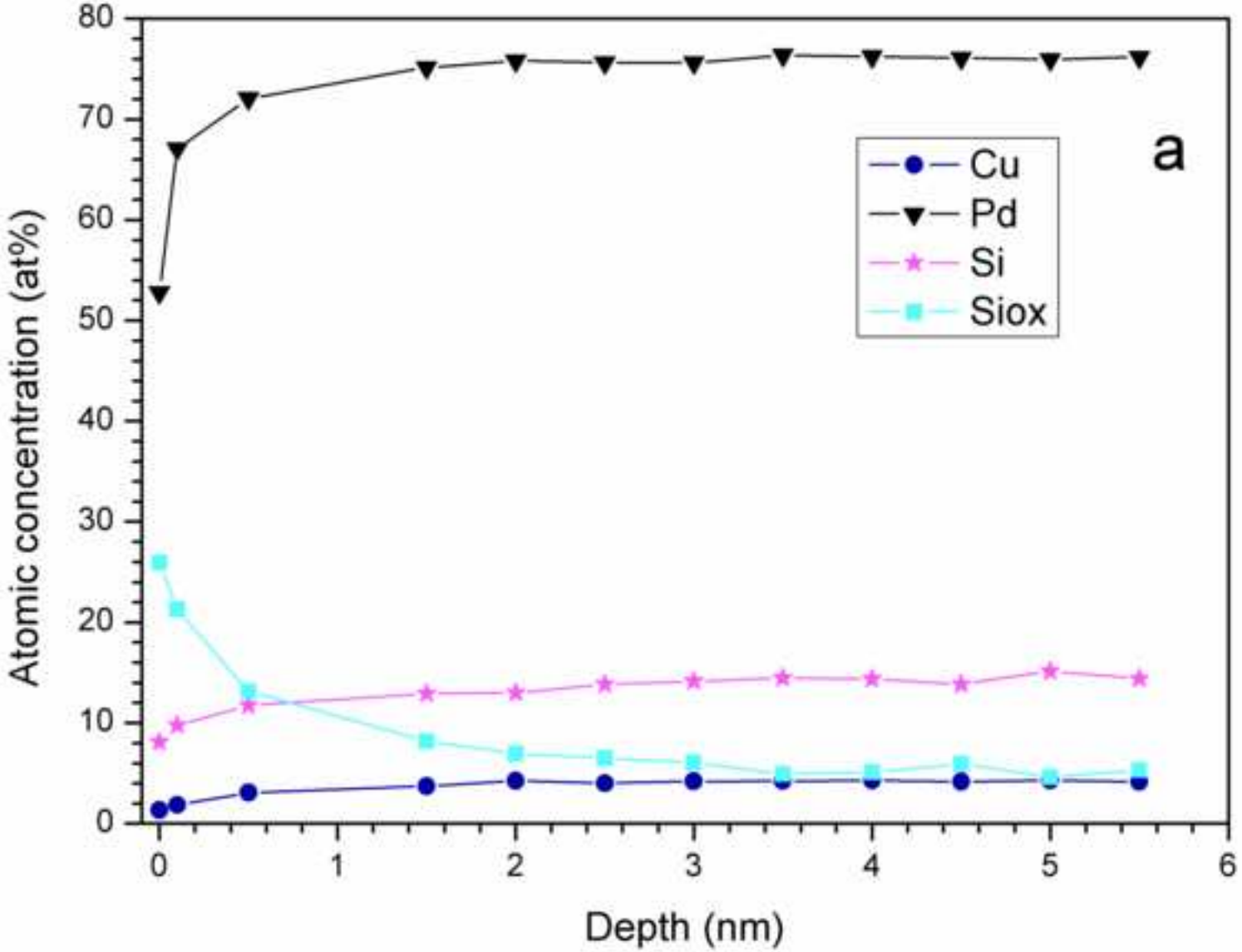
Atomic concentration (at%)
Depth (nm)
Cu
Pd
Si
Siox
a
0
10
20
30
40
50
60
70
80
0
1
2
3
4
5
6

Figure 5b

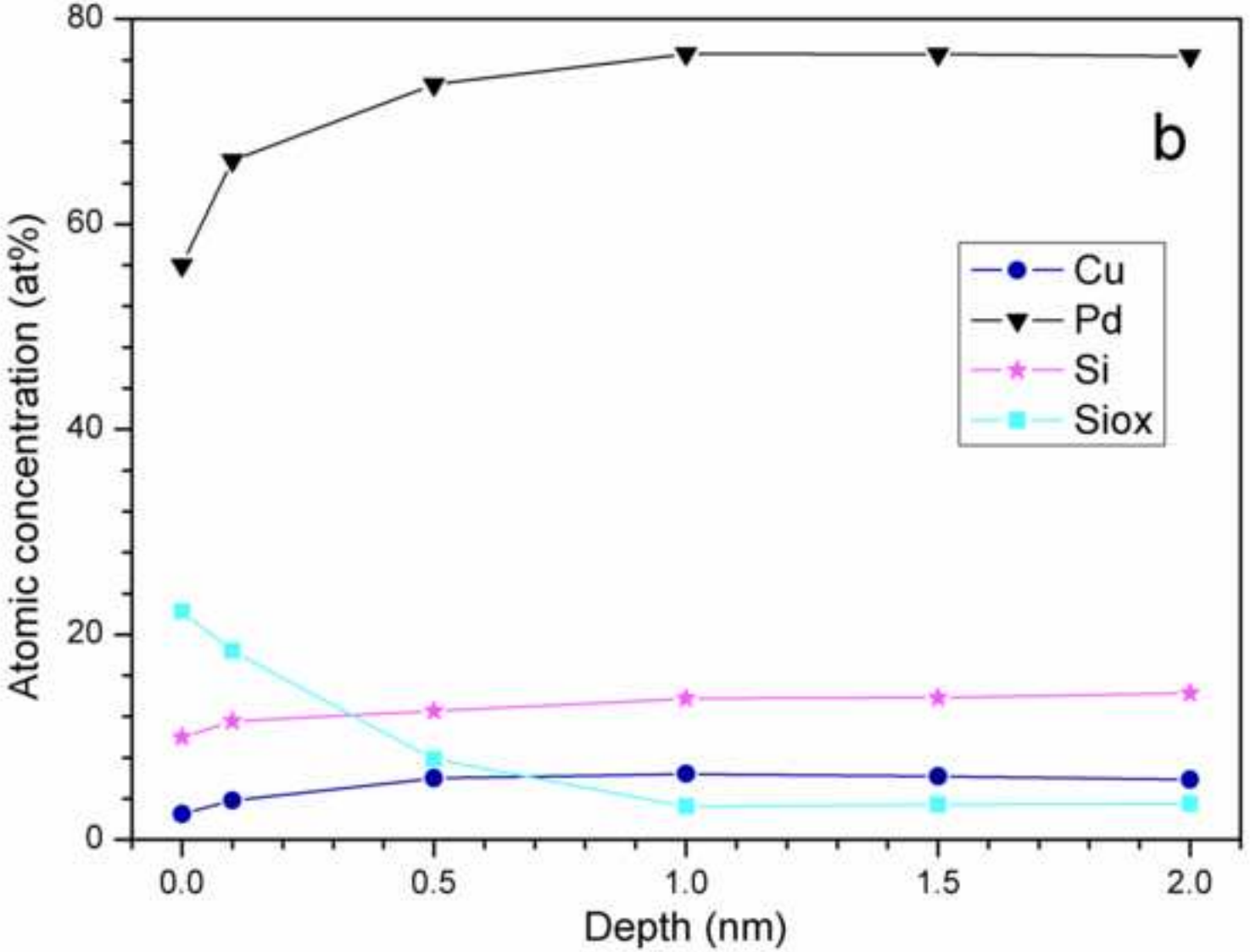
b
Cu
Pd
Si
Siox
Atomic concentration (at%)
Depth (nm)
0
20
40
60
80
0.0
0.5
1.0
1.5
2.0

Figure 5c

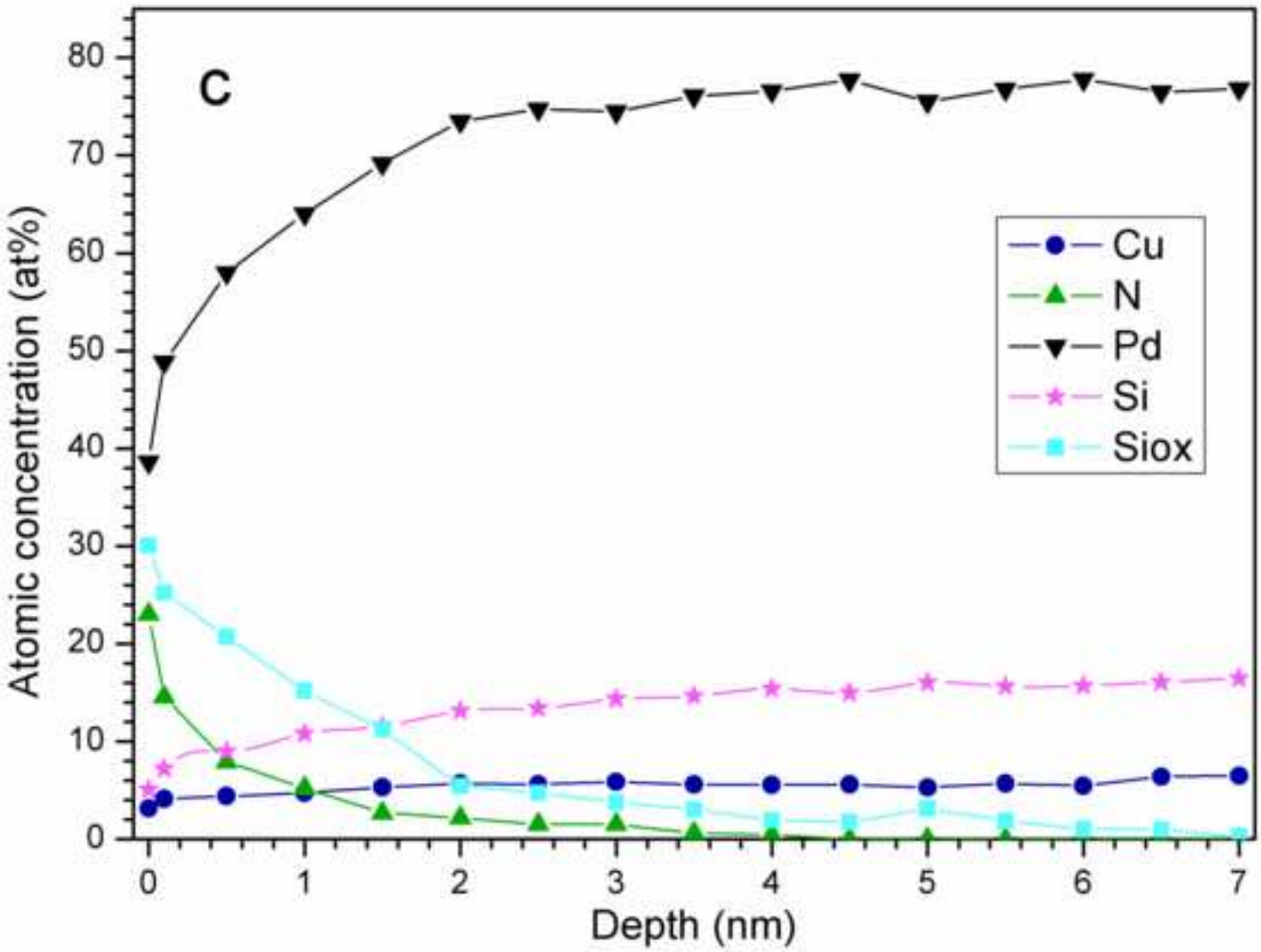
C
Atomic concentration (at%)
Depth (nm)
Cu
N
Pd
Si
Siox
0
10
20
30
40
50
60
70
80
0
1
2
3
4
5
6
7

Figure 5d

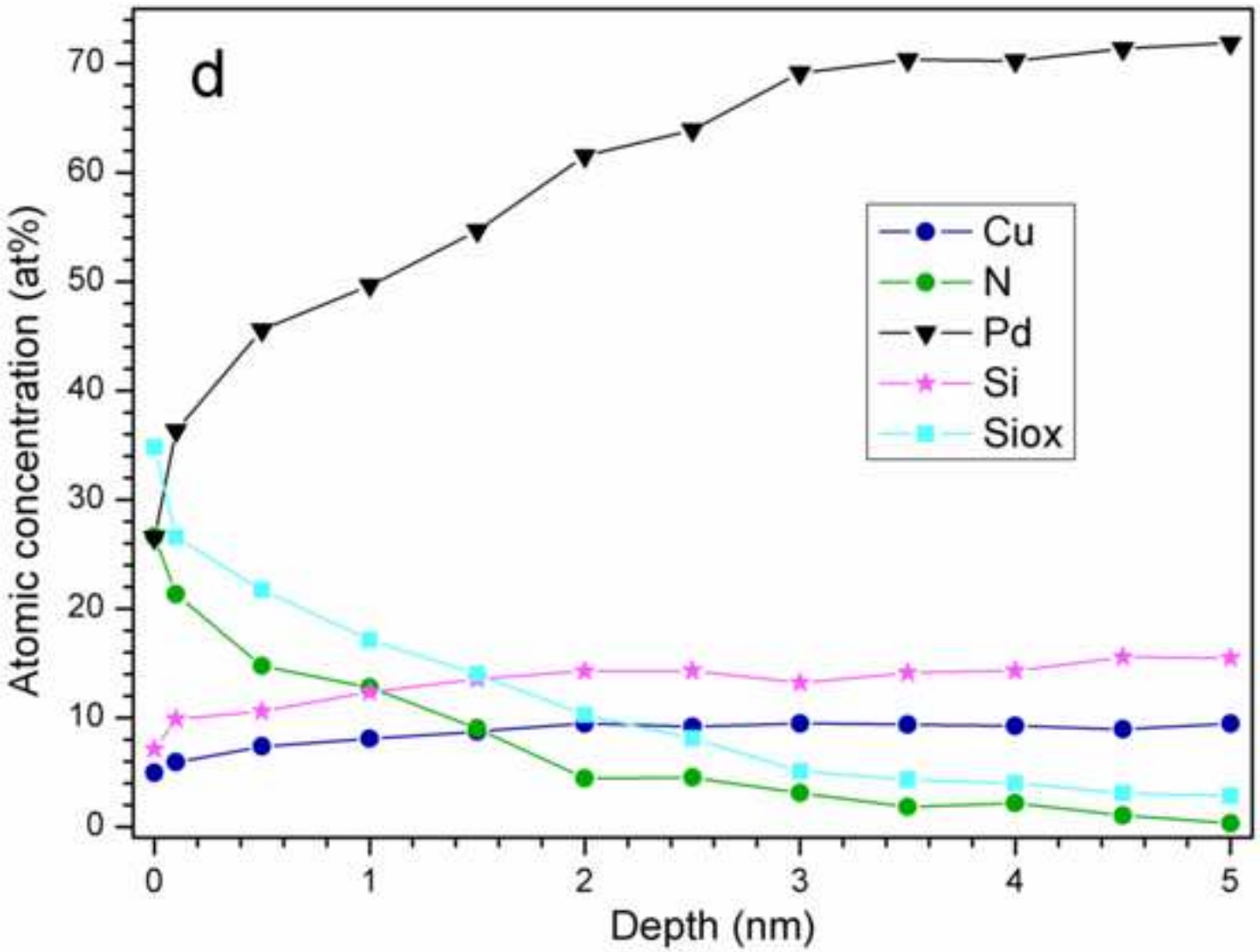
d
Atomic concentration (at%)
Depth (nm)
Cu
N
Pd
Si
Siox
0
10
20
30
40
50
60
70
0
1
2
3
4
5

Figure 6a

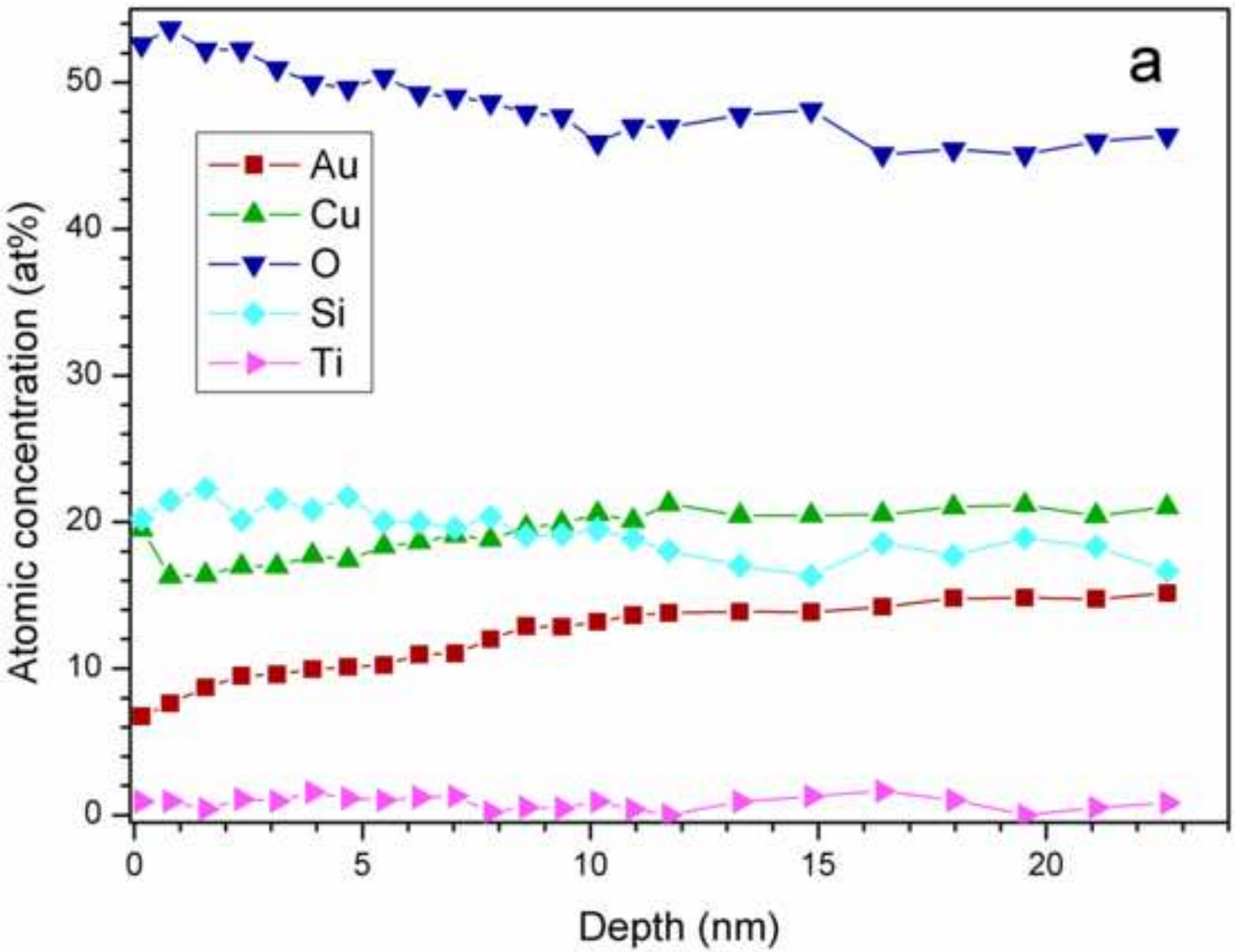
a
Au
Cu
O
Si
Ti
Atomic concentration (at%)
Depth (nm)
0
10
20
30
40
50
0
5
10
15
20

Figure 6b

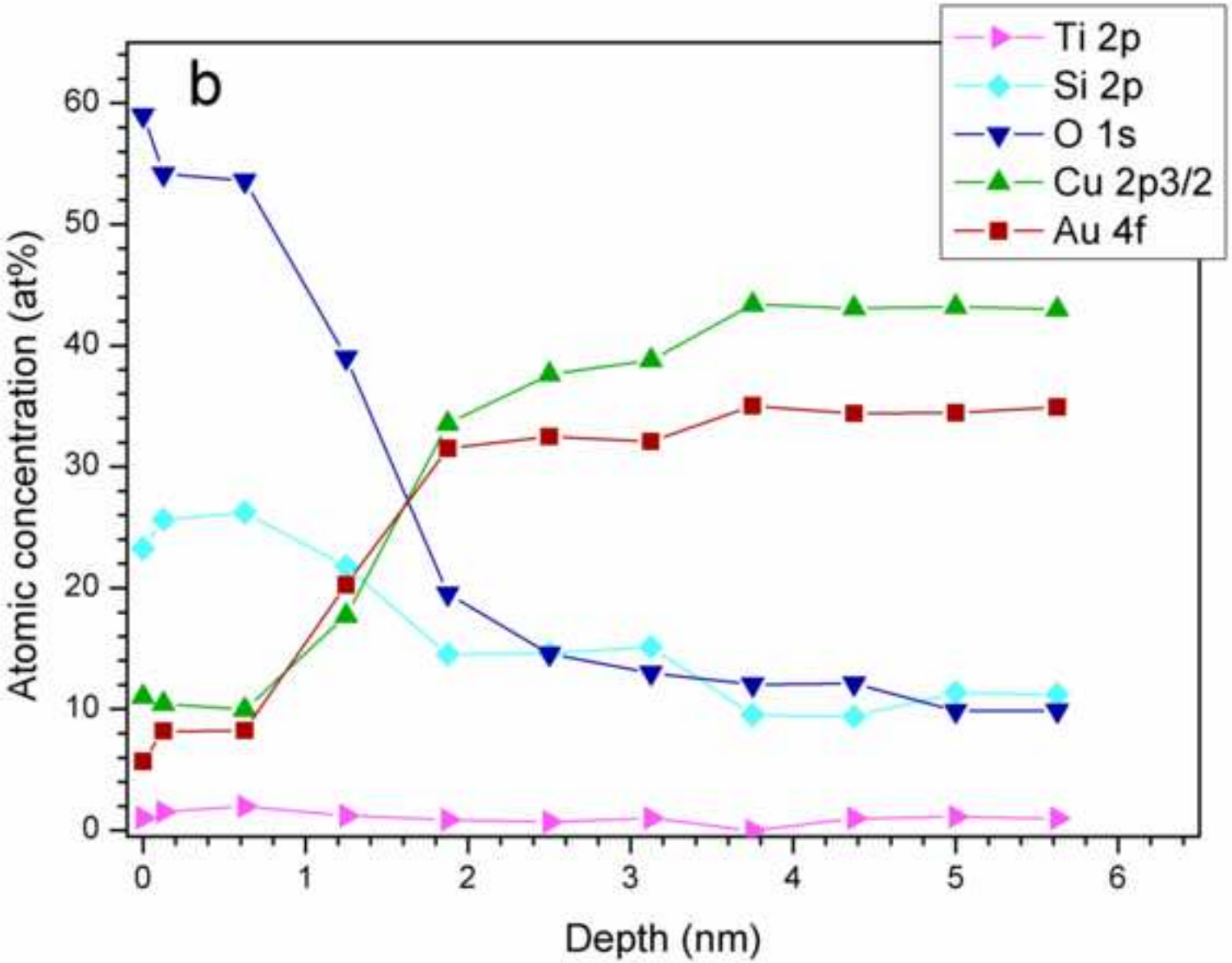
b
Ti 2p
Si 2p
O 1s
Cu 2p3/2
Au 4f
Atomic concentration (at%)
Depth (nm)
0
10
20
30
40
50
60
0
1
2
3
4
5
6

Table 1

Ion	Detection limit in nitric acid solution (0.2 M) in ppb (by mass)
Cu	20
Ni	20
Ti	10
Si	10
Au	100
Pd	100
Ag	100
P	100

Table 1 Detection limits of the ions analyzed by ICP-AES in nitric acid solution (0.2 M) expressed in ppb (by mass).